The Micromechanics of the Superficial Zone of Articular Cartilage

Running title: micromechanics of superficial zone cartilage

Authors: Jessica C Mansfield[1*], James S Bell[1] and C Peter Winlove[1]

[1]College of Engineering Mathematics and Physical Sciences, University of Exeter, UK

[*]Corresponding author:

email: j.c.mansfield@exeter.ac.uk

Address: Dr Jessica Mansfield, School of Physics, University of Exeter, Stocker Rd, Exeter, EX4 4QL, UK,

Phone: +441392723655

Abstract:

Objective: To investigate the relationships between the unique mechanical and structural properties of the superficial zone of articular cartilage on the microscopic scale.

Design: Fresh unstained equine metacarpophalangeal cartilage samples were mounted on tensile and compressive loading rigs on the stage of a multiphoton microscope. Sequential image stacks were acquired under incremental loads together with simultaneous measurements of the applied stress and strain. Second harmonic generation was used to visualise the collagen fibre network, while two photon fluorescence was used to visualise elastin fibres and cells. The changes visualised by each modality were tracked between successive loads.

Results: The deformation of the cartilage matrix was heterogeneous on the microscopic length scale. This was evident from local strain maps, which showed shearing between different regions of collagen under tensile strain, corrugations in the articular surface at higher tensile strains and a non-uniform distribution of compressive strain in the axial direction. Chondrocytes elongated and rotated under tensile strain and were compressed in the axial direction under compressive load. The magnitude of deformation varied between cells, indicating differences in either load transmission through the matrix or the mechanical properties of individual cells. Under tensile loading the reorganisation of the elastin network differed from a homogeneous elastic response, indicating that it forms a functional structure.

Conclusions: This study highlights the complexity of superficial zone mechanics and demonstrates that the response of the collagen matrix, elastin fibres and chondrocytes are all heterogeneous on the microscopic scale.

Keywords: second harmonic generation, two photon fluorescence, articular cartilage, micromechanics, elastin

Introduction:

Articular cartilage forms a low friction shock absorbing layer at the ends of bones in synovial joints. It contains few cells and consists mainly of a highly hydrated proteoglycan gel constrained within a network of type II collagen [1]. Cartilage structure changes with depth from the articular surface and is classified into three zones (superficial, transitional and deep) based on the organisation and degree of alignment of the collagen fibres (figure 1) [1, 2].

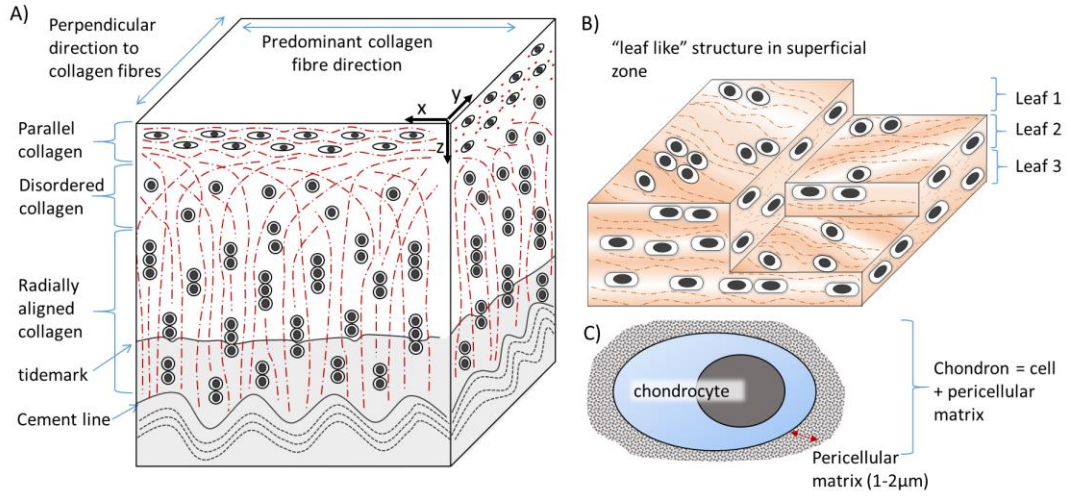

Figure 1. Schematic diagrams to show the change in cartilage structure with depth (A), the leaf like structure at the surface (B) and a chondron (C)

The superficial zone has several distinct structural features and we are interested in the role these play in its unique mechanical properties. In this zone, the collagen fibres are aligned parallel to the articular surface compared to the perpendicular fibres in the deep zone (figure 1). The proteoglycan content and fixed charge density are lower than in the deep tissue [3, 4]. In addition it contains an extensive network of elastin fibres which are roughly aligned with the collagen fibres in the plane parallel to the surface [5-9]. Their role is completely unexplored and is therefore a target of this investigation. The superficial zone chondrocytes are morphologically different, being disc shaped in the plane parallel to the articular surface unlike the more spherical chondrocytes in the deeper zones. Their pericellular matrix [10] also differs, with both elastin [7] and lipids [11] being present only in the superficial zone pericellular matrix. They also have metabolic differences with a lower rate of proteoglycan and protein synthesis than in the deeper zones [12] and a different metabolic response to tensile loading [13].

The bulk mechanical properties of this zone of cartilage are reasonably well defined. It has a lower compressive modulus than the deeper tissue [4] resulting in more matrix deformation and larger changes in chondron volume [14] under compressive load. Its high water content [15] and permeability result in interstitial fluid being exuded into the joint cavity under minimal compressive loading [16] which is important to joint tribology [17].

Although tensile loads are not generally considered to be physiological, Neu et al [18] demonstrated that compressive loading gives rise to tensile forces parallel to the surface in the superficial zone cartilage. Previous tensile testing studies demonstrated that the tensile modulus is largest in the direction parallel to the predominant collagen fibre orientation [19-21], and the tensile modulus decreases with depth, with the superficial zone being up to 5 times stiffer than the deep zone [20-22]. The tensile properties vary across joints in line with loading patterns *in vivo* [23] and the tensile modulus decreases with fibrillation, osteoarthritic degeneration [23] and age [24, 25]. Collagen fibres are able to support very high tensile loads and under compressive loading the applied pressure, coupled with osmotic swelling generated by the proteoglycans is arrested by tension in the collagen fibres, preventing lateral over-expansion. Under transient loading conditions the proteoglycans also play a role in determining the rate of redistribution of interstitial fluid [24].

In this study we combine microscopic observations with mechanical loading to look at the microstructural response of cartilage to both compressive and tensile loads. This was made possible through the use of two multiphoton microscopy techniques; two-photon fluorescence (TPF) and second harmonic generation (SHG). TPF differs from single photon fluorescence as the flourophores are excited by the simultaneous absorption of 2 infrared photons instead of a single visible photon [26]. In cartilage, endogenous fluorescence provides contrast for the cells and elastin fibres [5, 7]. In SHG 2 infrared photons are simultaneously absorbed and a single visible photon is emitted at exactly half the original wavelength and this only occurs in highly ordered crystalline materials which lack inversion symmetry [27]. In cartilage, SHG reveals the collagen matrix [5, 28, 29]. Like confocal microscopy they allow 3D imaging at submicron resolution. They avoid the need for sectioning, fixing or staining of the sample making them ideal for imaging in mechanical studies as the material properties should remain unaltered [21, 30-33]. This work builds upon a previous study using TPF to investigate the response of articular cartilage to tensile load, which revealed unexpected heterogeneity in the microscopic strain fields [21].

We first investigate the elastic moduli and Poisson's ratios of the superficial zone under tensile and compressive loads, taking advantage of multiphoton microscopy to measure their micron-scale variations in fresh tissue. We then investigate the microstructural bases of these properties, paying particular attention to the behaviour of the elastin fibres and cells. Finally we discuss the effect of early degenerative changes.

Methods:

Tissue Preparation:

Thoracic legs from 16 horses aged 3-14 years were obtained from a local abattoir (Potters, Taunton). Horses older than 14, skeletally immature or lame were excluded from the study. The metacarpophalangeal joints were opened and cartilage plugs were removed from the proximal phalanx within 3 hours of euthanasia. 10 samples were used for tensile testing and 6 for compressive loading. As cartilage is stiffer when strained parallel to the predominant collagen fibre direction, cartilage strips were taken both parallel and perpendicular to the predominant collagen fibre orientation as defined by split line measurements (see supplementary information) in order to fully characterise its tensile properties in this plane.

Multiphoton microscopy:

SHG and TPF were excited using the 810nm output of a Ti:Sapphire laser (Mira 900 Coherent) with 100fs pulses and a 76MHz repetition rate.

For the tensile loading experiments, we imaged with a modified, non-inverted confocal laser scanning microscope (FluoView 300 and BX51 Olympus UK) with a 1NA 60x long working distance dipping lens (LUMPLFLN 60XW Olympus UK). For the compressive loading experiments, we imaged with a modified inverted confocal laser scanning microscope (FluoView 300 and IX71 Olympus UK) with a 1.2NA 60x objective (UPlanSApo Olympus UK).

For both experiments, SHG and TPF were collected simultaneously in the epi-direction. The signal was separated from the laser fundamental by a long pass dichroic filter (670dcxr Chroma technologies) and a colour glass filter (CG-BG-39 CVI laser) and the SHG and TPF were directed onto two separate photomultiplier tubes (PMTs) (R3896 Hamamatsu Japan) by a long pass dichroic filter

(Semrock Di02-R405). Additional filters were placed in front of the PMTS (Semrock FF01-405/10 and Semrock FF01-520/70 for SHG and TPF respectively).

To avoid photodamage the average laser power at the sample was maintained below 20mW.

Mechanical loading:

For tensile loading (figure 2A), strains were applied using micrometers accurate to 10µm (MT1/M Thorlabs) and the corresponding load was measured with a 5N force transducer (model 31 RDP Electronics) connected to a data logger (Picoscope 2015). Cartilage strips (approximately 0.8 x 0.5 x 10 mm) were attached between two metal paddles using superglue gel leaving 5mm of cartilage free for tensile loading. Multiphoton imaging was carried out at a series of strains between 0 and 12%. Tensile strains of up to 7% have been found to be physiological [18] and the higher strains probe the connectivity of the extracellular matrix fibre networks.

For compressive loading (Figure 2B), a micrometer drove a 15mm diameter platen against a 12mm diameter cartilage plug supported on a stainless steel plate containing a 10mm diameter coverslip-covered window. Between the cartilage and the platen was a 444N compression load cell (model 13 RDP Electronics) connected to a data logger to measure the applied force. Pressures between 0 and 400kPa falling within the normal physiological range were applied.

During all loading experiments the samples were kept immersed in phosphate buffered saline, pH 7.4. The bath was covered to avoid evaporation and changes in ionic concentration which would change the mechanical properties of cartilage [23]. Images were taken after the sample had equilibrated for 30minutes.

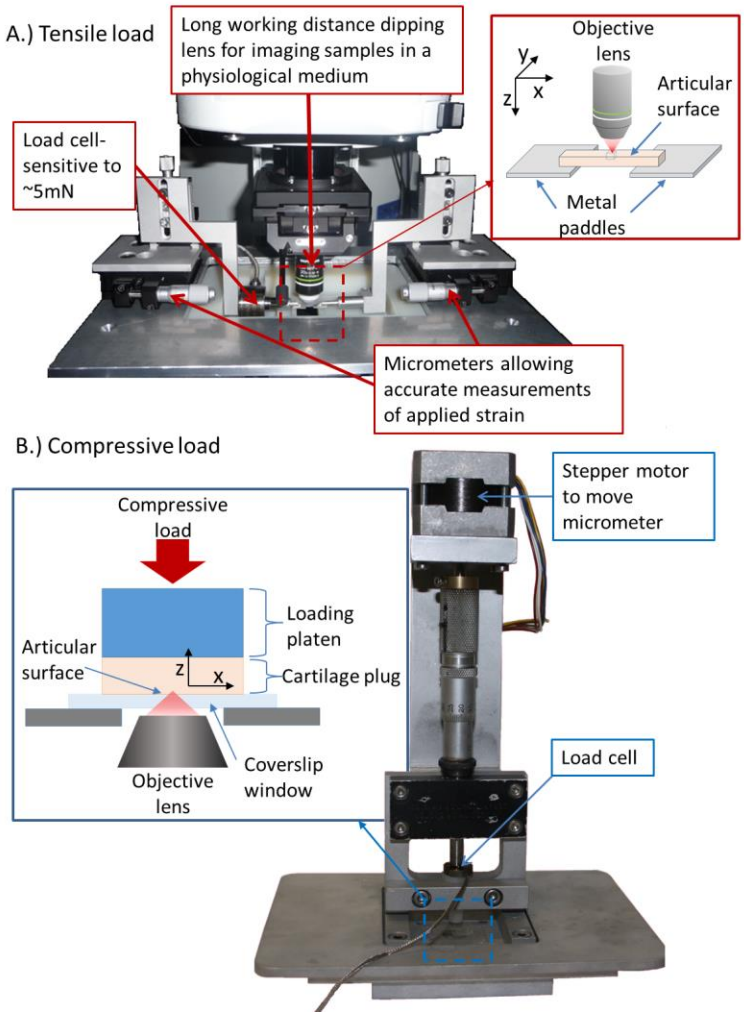

Figure 2. Experimental rigs for tensile loading (A) and compressive loading (B).

Data analysis:

Image stacks were taken through the superficial 100µm of articular cartilage under both compression and tensile load. To act as a fiducial marker, a square was photobleached into the sample at a depth of 20µm in the plane parallel to the articular surface. As the sample was strained the changes in dimensions of the square were used to calculate local strains and Poisson's ratio ($\nu = \varepsilon_{\perp} / \varepsilon_{\parallel}$, with $\varepsilon_{\parallel}$ and $\varepsilon_{\perp}$ being the strains parallel and perpendicular to the applied load respectively) in this plane. Elastin fibres were visible in the TPF images as thin lines of brighter fluorescence and the chondrocytes appeared as darker (<70% average matrix intensity) ellipsoids. Images were analysed using ImageJ [34]. Overlays were used to track the movements of individual cells and elastin fibres between image stacks taken at progressive strains (figure 3). Under mechanical loads cells can be displaced and change shape. Displacement, taken as an indicator of the local strain field, was measured using a cell tracking algorithm we have reported previously [21, 35]. Ellipses were fitted to

the cell boundaries in the TPF images in the *x y* plane; from these changes in aspect ratio and reorientation of the principal axis were measured. Out of plane distortions were found to be minimal.

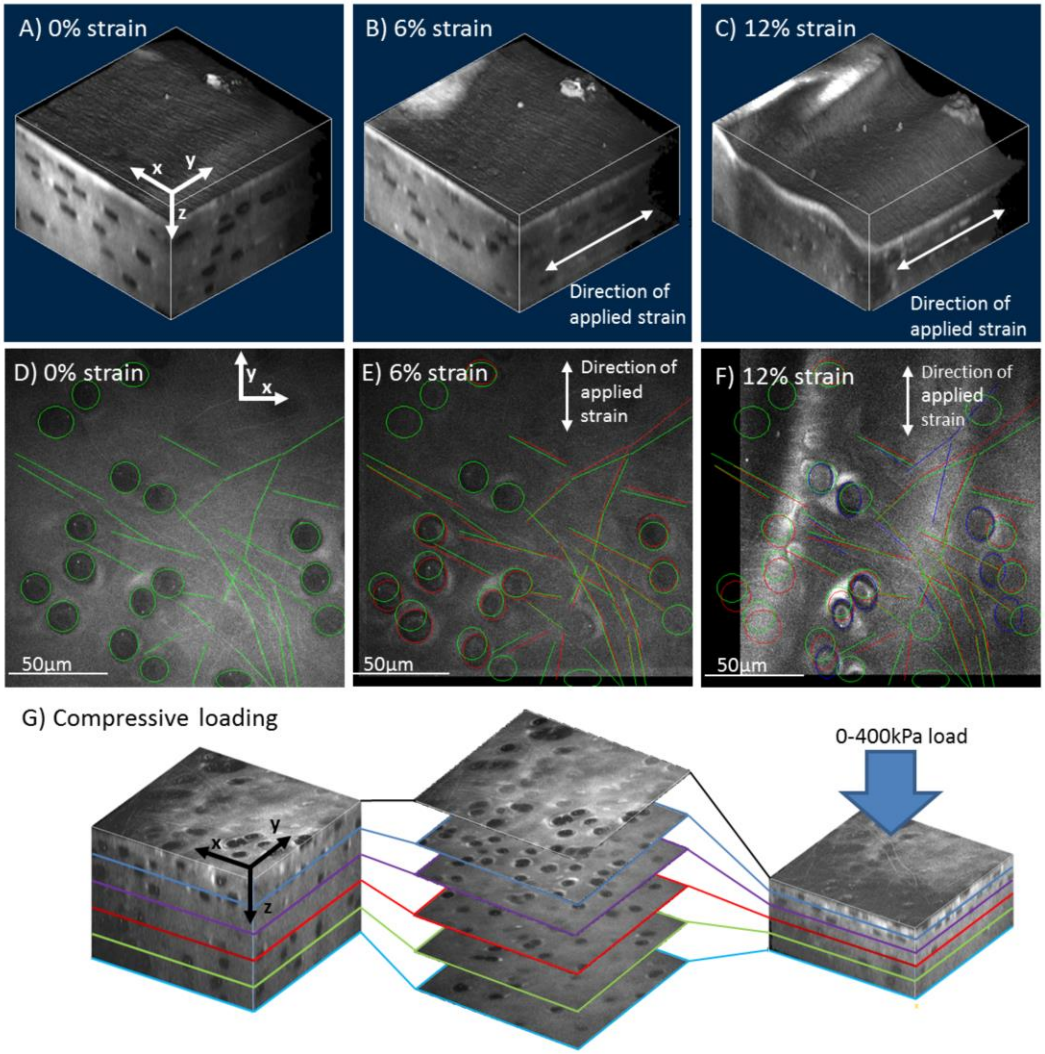

Figure 3. A-C) 3D reconstructions of data stacks taken at increasing tensile loads (sample strained perpendicular to collagen fibre direction) D-F) individual images from each image stack containing an overlay demonstrating the cellular features and elastin fibres which were tracked between progressive strains. G) image stacks taken before and after the application of strain showing tracking of frames between stacks to give displacements in the z direction.

Results

Continuum Mechanics

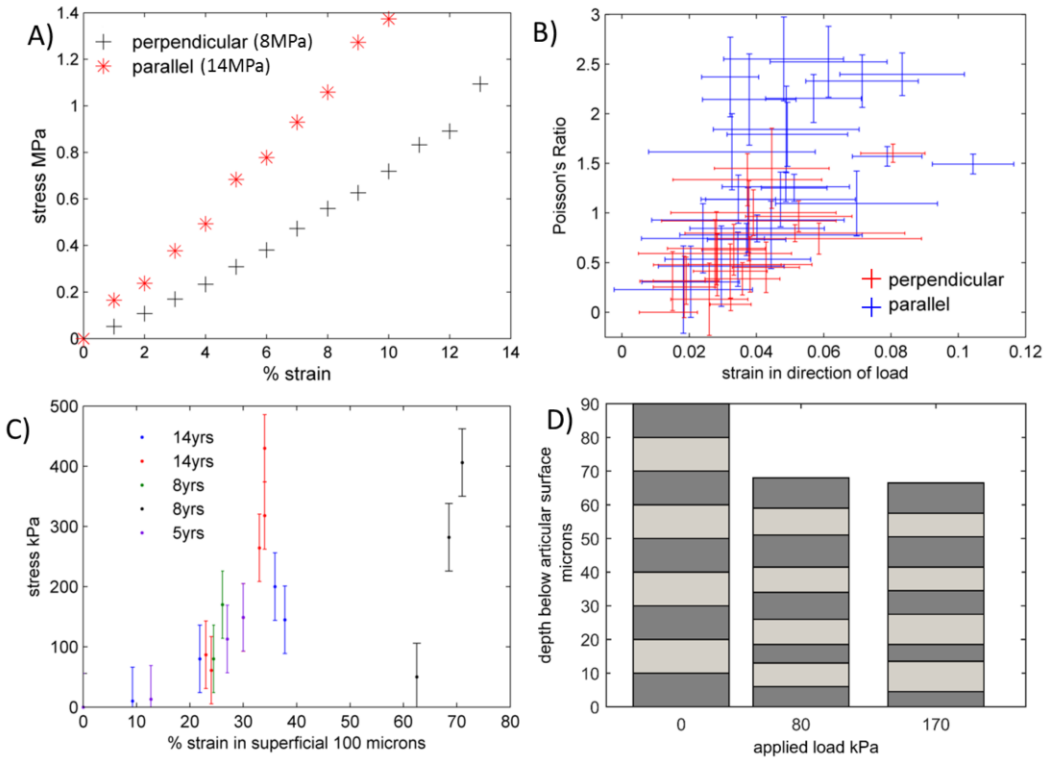

Figure 4. Stress-strain behaviour under tensile and compressive load. A) typical stress-strain graphs for paired samples tensile loaded parallel and perpendicular to collagen fibre direction B) x-y Poisson's ratios calculated from the bleached square in all tensile tested specimens (blue – load applied parallel to principal collagen direction , red – strain perpendicular). C) Overall strain in the z direction in the superficial 100µm as a function of applied compressive load. D) Variation of compressive strain with depth (the coloured bands represent 10µm depth sections of the unloaded image).

i. Tensile Modulus and Poisson's Ratio

Figure 4A shows representative stress-strain curves for samples strained parallel and perpendicular to the collagen fibre direction.

There is a large variation in the Poisson's ratios for a given strain, which demonstrated heterogeneity in mechanical properties on this scale, however over the range of strains investigated the Poisson's ratio increased with strain (figure 4B). From the correlation coefficient we were able to reject the Null hypothesis that there was no correlation between tensile strain and Poisson's ratio ($p < 0.01$). It is also higher in samples strained parallel to the collagen fibres compared to those strained perpendicular; a student t-test was performed and we rejected the Null hypothesis that there was

no difference between the parallel and perpendicular samples ($P < 0.05$). Poisson's ratios greater than 0.5 for tensile loading indicate water being extruded from the cartilage, with higher Poisson's ratios corresponding to greater water loss.

Compressive Modulus and Poisson Ratio

The mean unconfined compressive modulus of the most superficial 100µm as determined from the gradient of the stress/strain curve in figure 4C was a non-linear function of strain, increasing to 150-450kPa at 35% strain. One sample showed much greater compression at equivalent loads and we suspect that this sample was in an early stage of degeneration. Lateral expansion under compressive load was 1-2% at 38% strain, giving a Poisson's ratio of only 0.04. The accuracy of the strain measurements was insufficient to resolve differences in the strains in the x and y directions. The cells did not show any significant lateral displacement and remained in the same plane as their neighbouring cells, therefore the axial strain could be estimated by tracking the cells z-displacement. This showed a non-uniform distribution over the superficial 100µm (Figure 4D) with the greatest strain in the most superficial layers although the pattern of variation with depth is somewhat irregular.

Structural Responses to Tensile and Compressive Loading

i. Cellular Displacement and Local Strain Distribution

Tracking the movement of cells between strained and unstrained samples provides information on the local strain distribution. Our previous study [21] revealed heterogeneity of the tensile strain field on this scale, which, we argued, reflected the leaf-like organisation of the collagen matrix [36], illustrated in figure 1B, with adjacent leaves moving relative to each other as the tissue deformed. This behaviour is shown in Figures 5A and B. Under compressive loads chondrocyte displacement in the plane parallel to the surface was much smaller, 1-2% at a compressive strain of 38%. Additionally the strain distribution in this plane showed no clearly defined areas of higher or lower strain which could be related to leaves of collagen (figure 5C).

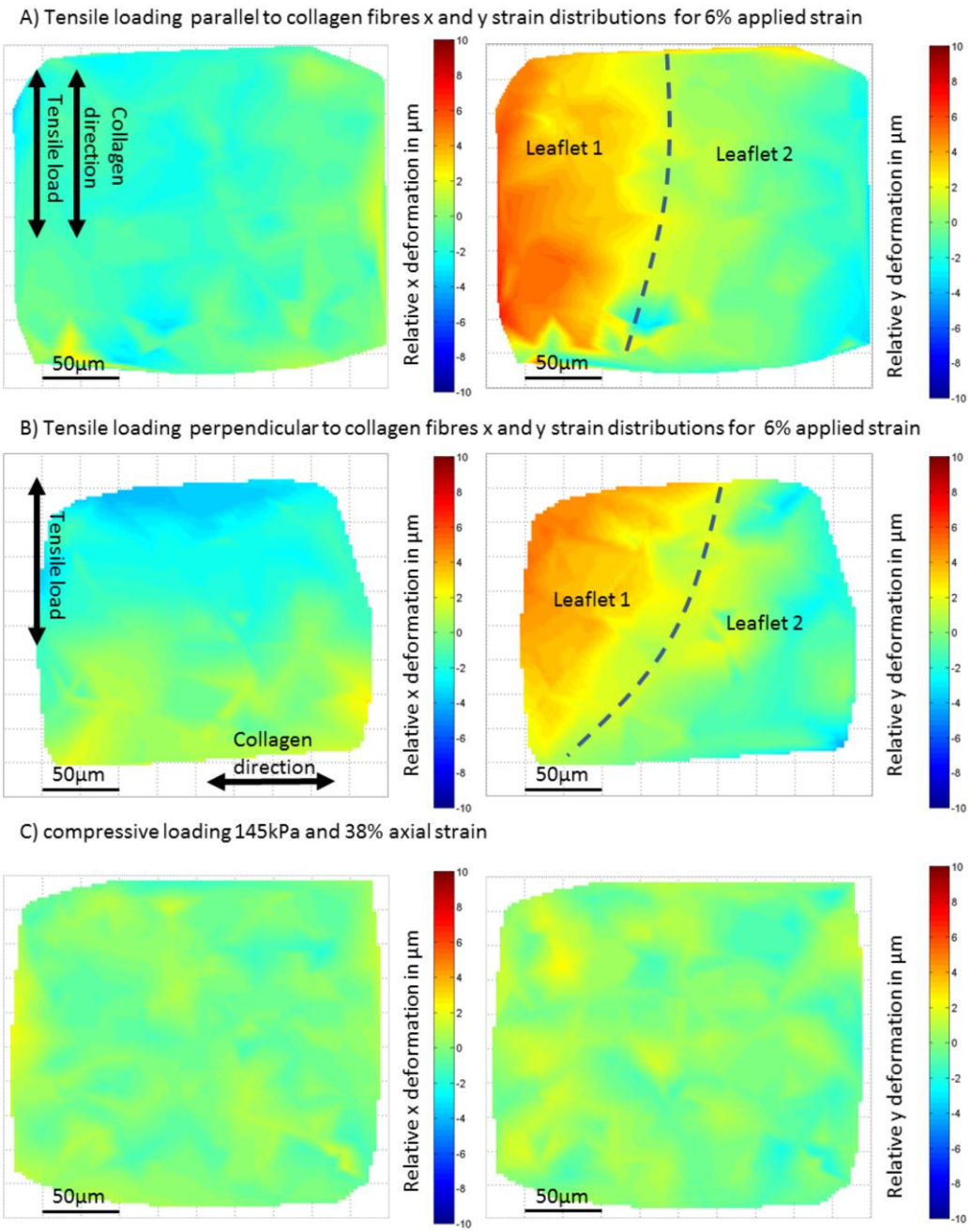

Figure 5. Local strain distributions in a plane parallel to the articular surface calculated from cell tracking measurements. A) Local x and y strain distributions at 6% strain, applied parallel to the predominant collagen orientation. B) x and y strain distributions at 6% strain applied perpendicular to the predominant collagen orientation. C) x and y strain distributions at a 38% compressive strain load

ii. Cell Deformation

Under tensile load the chondrocytes re-orientated and deformed in the *x-y* plane. Figures 6A and B show the response of all the cells (n=193) in a sample strained perpendicular to the collagen fibres. In the unloaded state the cells long axes were at approximately 25° from the direction of applied strain (mean angle 25.0°±36.7), but at 12% strain their long axes had rotated closer to the direction of applied strain (mean angle 15.6° ±29) (Figure 6A). At the same time, the aspect ratio of the fitted

ellipses increased from 1.3±0.2 to 1.5±0.3 (Figure 6B). Similar patterns of reorientation and deformation were observed in all samples strained both parallel and perpendicular to the collagen fibres however the exact values of the mean angles and aspect ratios were dependent on the original distribution of cell shapes in the region of interest. The response of the cells as a function of depth from the articular surface was also analysed however this showed no reliable pattern of depth dependence.

Under compressive load any reorientation or changes in ellipticity in the *x*-*y* plane were too small to be resolved. However, there were large changes in the thickness of cells (Figure 6C). At a load of 145 kPa, which produced an overall strain of 38% the median cellular compressive strain was 46% (Figure 6D), although there was considerable variation in the response of individual cells. Assuming 1.5% strain along the other axes (measured from either cell tracking or the bleached square) and that the cells are represented by elliptical cylinders (with an elliptical cross-section in the x-y plane and a cylindrical profile in the z direction) this represented a volume decrease of 44% compared to the total change in volume of the imaged field of 36%.

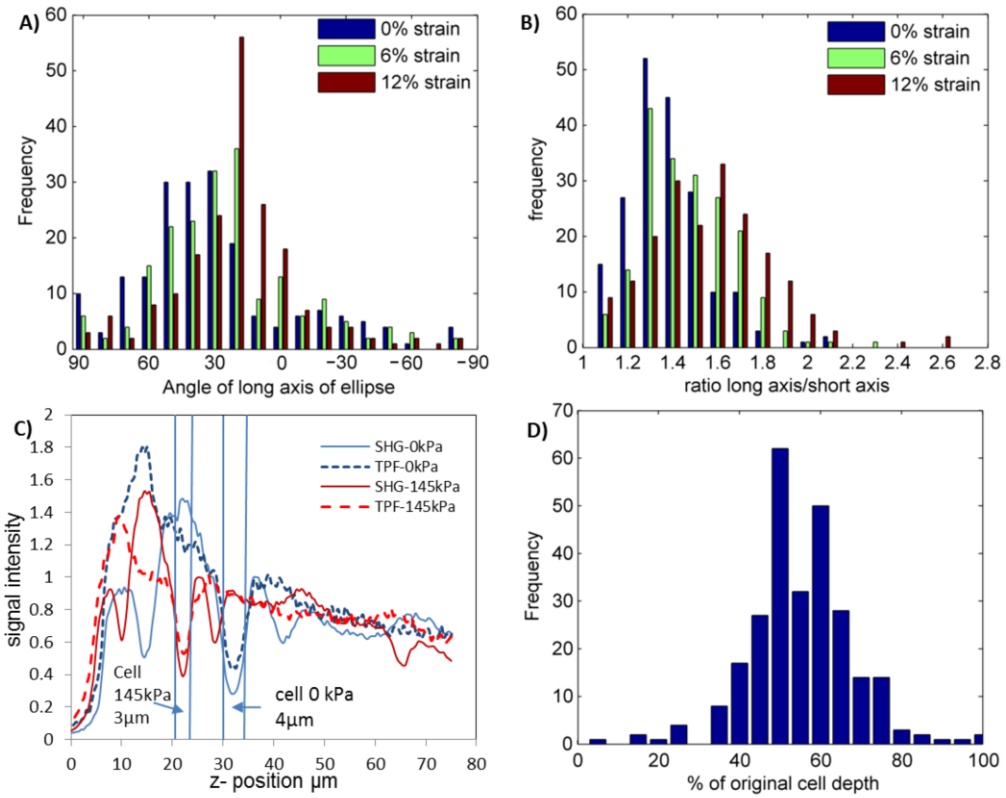

Figure 6. Cellular responses to compressive and tensile loads. A) Changes in cell angle under tensile load, the distribution of the long axis of the ellipse fitted to the cell (90° corresponds to the direction of applied strain) B) Changes in the ratio of long to short axis of the cellular ellipse under tensile strain. C) TPF and SHG signal intensity profiles in the z-direction across an individual cell under zero load and 145 kPa compressive load (resulting in a mean strain of 38% in the top 100µm of tissue). Both signals show a dip in intensity at the cell boundaries which can be used to measure both cellular displacement and changes in the z-thickness of the cells. The boundary was taken as the 70% intensity contour. D) Change in cell thickness for individual cells as the load is increased from 0 to 145kPa.

iii. Elastin fibres:

Previous studies revealed long, straight elastin fibres running approximately parallel to the articular surface and the predominant collagen fibre direction in the superficial zone cartilage [5, 7]. In the proximal phalanx cartilage investigated here these fibres appeared to separate into two distinct populations (figure 7A) with a dense population of fibres with a highly parallel alignment at the articular surface (top 2µm) (figure 7B) and a less dense elastin network with a wider range of fibre angles (although still loosely correlated to the split line direction) in the cartilage beneath (figure 7C).

Because the alignment of the fibres in the z-direction may influence their response to load the range of fibre angles was analysed. As the depth of focus is known, the angle of the elastin fibres with respect to the x-y plane was calculated from their apparent length within this plane. This was 3.2°±2.4° (n= 350 fibres), and was considered to be too small to affect the analysis presented below.

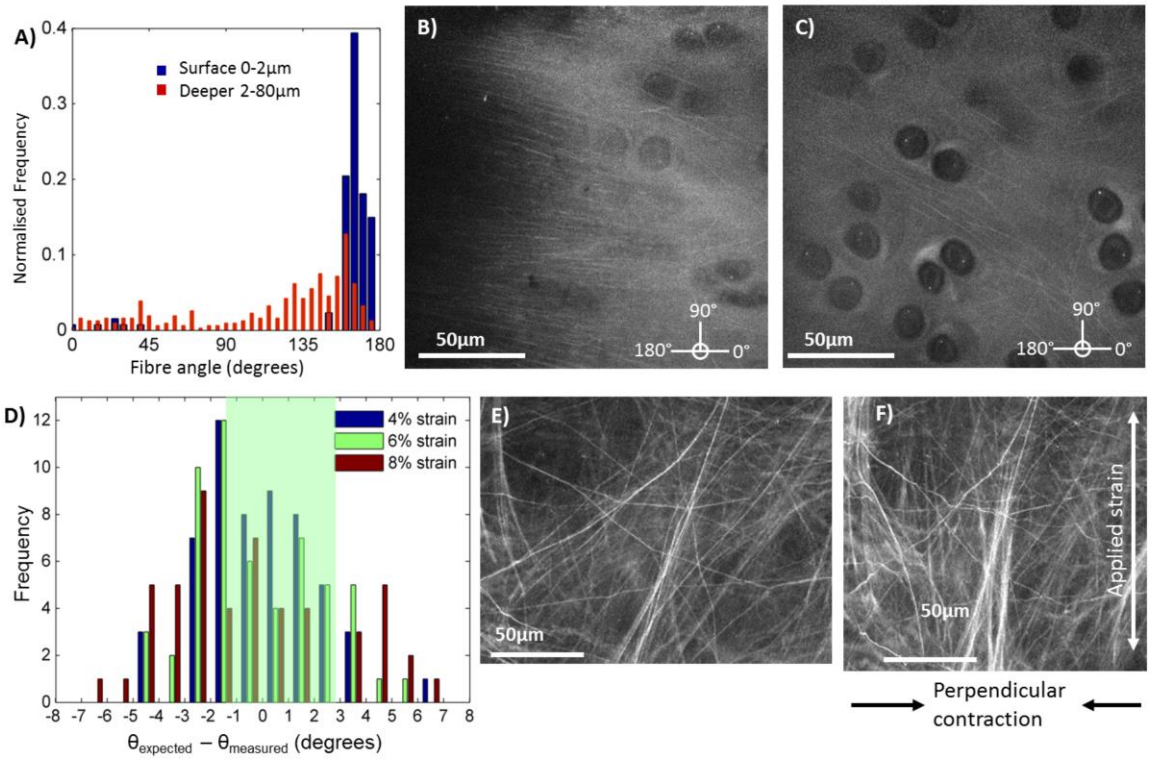

Figure 7. Superficial zone elastin fibres and their response to strain. A-C) variations in elastin fibre organisation with depth in unloaded cartilage A) histogram of elastin fibre angles comparing the most superficial 2µm and the deeper fibres within a stack. TPF images of elastin fibres at the articular surface (B) and 20µm below the articular surface (C). D) Comparison of measured and predicted changes in elastin fibre angles in a sample taken from 0-8%strain (green shaded area shows values which agree with the prediction within the bounds of uncertainty – positive values fibre has aligned more in direction of strain than predicted – negative values fibre has aligned less in direction of strain than predicted). E and F) TPF images of superficial fibres before (E) and after (F) a large applied strain. In (F) some fibres have crimped in the direction perpendicular to the applied strain – demonstrating the relief of prestress within the sample.

Response to load:

We sought to establish whether the reorientation of the elastin fibres under tensile load followed the changes in the strain field of the surrounding matrix: any disparity would suggest longer-range connectivity (greater than the 250μm field of view) between fibres or with other matrix components thereby suggesting a mechanical role. Assuming that the surrounding matrix is homogeneous (an assertion that is likely to be overly simplistic) and linearly elastic, that force is continuous across the fibres and there is no slip between fibre and matrix the predicted change in fibre angle is given by the equation:

$$\tan \Theta' = \left(\frac{\varepsilon_{\parallel}+1}{\varepsilon_{\perp}+1}\right) \tan \Theta \qquad (1)$$

Where Θ and Θ' are the unstrained and strained fibre angles respectively and $\varepsilon_{\perp}$ and $\varepsilon_{\parallel}$ are the tissue strains perpendicular and parallel to the load as calculated from the deformation of the bleached square marker. The difference between the measured and predicted elastin fibre angles for a sample strained incrementally to 8% perpendicular to the predominant collagen orientation is shown in figure 7D. This shows that many fibre angle changes disagreed with the model to an extent that exceeded the uncertainty in the measurements (±2°calculated from repeated measurements on individual fibres). Elastin fibre tracking was performed on 6 samples and the percentage of angle changes disagreeing with the model ranged between 25% and 67%. We therefore conclude that the elastin fibres are part of a functional network. Furthermore, our results suggest that the elastin fibres are under strain even in the unloaded state. First, the fibres are likely to have a very low bending modulus but are remarkably straight. Secondly, the behaviour of elastin fibres aligned perpendicular to the direction of applied tensile strain indicated prestress, as in samples with contractions of up to 15-17% in the perpendicular direction the elastin fibres still remained straight, although in some samples showing greater relaxation, the elastin fibres were observed to crimp as illustrated in figure 7E and F. This suggests that in the intact tissue the elastin fibres are under a strain of at least 15%.

Under compressive load no deformation or movement of the elastin fibres was observed, reflecting the fact that the fibres lay in the x-y plane (data not shown).

iv. Surface Corrugations

At high tensile strains (≥ 8%) ridges appeared at the articular surface. These were parallel to the direction of applied strain, irrespective of the orientation of the collagen network. However, the

ridges were wider and deeper in the samples strained perpendicular to the predominant collagen direction (peak to peak distance 65±20µm and depth 8±3µm compared to 17±7µm and 3.5±2µm in the parallel samples at 12% strain), as shown in the representative image stacks in figure 8. Similar ridges were observed by Sasazaki et al [37], and multiphoton microscopy now allows us to visualise the 3D topology at progressive strains and the behaviour of the underlying cells and fibres. In samples strained perpendicular to the elastin/ collagen fibre direction the elastin fibres clearly followed the surface topology. The cellular displacements at the articular surface were more complicated, figures 8C and D show a group of 5 cells which appear to have been pulled together at the location of a ridge. Deeper within the cartilage the cellular displacements are more regular indicating that the effects of the corrugations are dissipated over a depth of approximately 30µm.

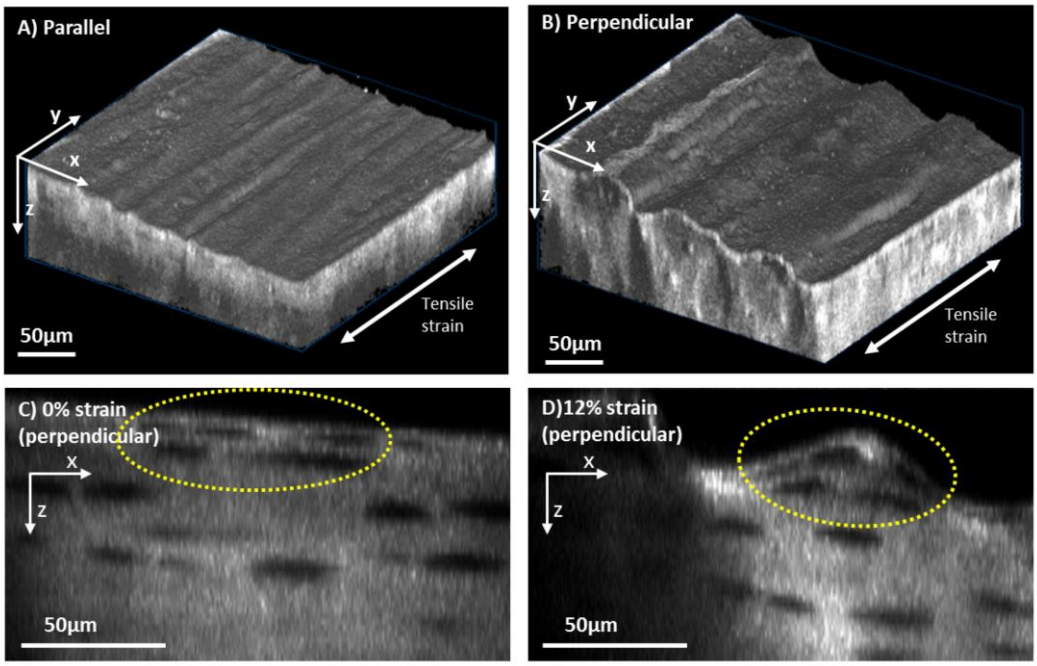

Figure 8. Surface corrugation at high strains. A) 3D reconstruction of a sample at 10% strain parallel to the collagen fibre direction B) Contiguous cartilage sample at 10% strain perpendicular to the predominant collagen fibre direction. C and D) Transvers sections from a perpendicular sample at the same site at zero and 10% strain. Highlighted region indicates 5 cells near the surface showing large displacements under strain.

v. Early Degenerative Changes

Although cartilage samples were from horses with no known history of lameness and no lesions visible to the naked eye, in two cases tensile testing and microscopy revealed abnormalities which may represent the earliest stages of osteoarthritic degeneration. In these samples the overall tensile modulus fell within the normal range, but the microscopic strain in the image field was lower than the total strain applied suggesting that regions of higher strain occurred elsewhere. In samples

strained perpendicular to the collagen fibre direction splits were observed originating from the articular surface. These first became evident at 6% strain with additional splits becoming evident at larger strains (figure 9) and were perpendicular to the applied strain and parallel with the collagen fibre direction. Their depth ranged from 15-20µm for the largest split to about 2µm for the smallest splits. In these specimens the Poisson's ratio was lower than in regions showing no abnormalities (<0.6), consistent with stress relief associated with split formation. In samples strained parallel to the collagen fibre direction surface splits did not form and the Poisson's ratio was within normal bounds.

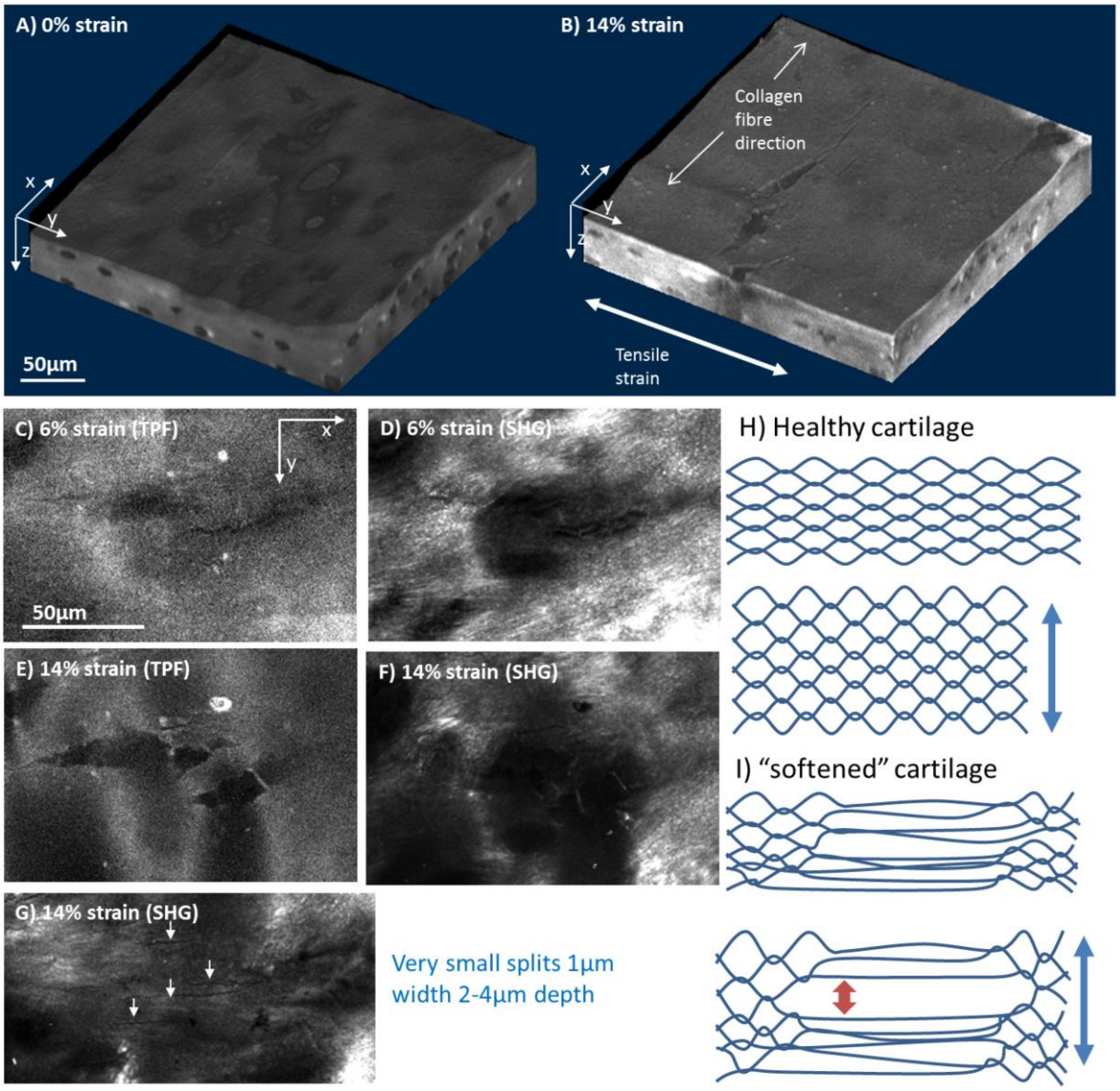

Figure 9. Response of early degenerate cartilage to tensile loading perpendicular to the collagen fibre direction. A) and B) 3D reconstructions at 0 and 14% strain showing split formation perpendicular to the direction of applied strain and parallel to the collagen fibre direction. C) and D) higher magnification images of the split at 6% strain. E) and F) higher magnification images of the split at 14% strain. G) SHG image showing additional smaller splits in the collagen network. H,I) Schematic diagrams of the suggested response cartilage to tensile load perpendicular to the collagen fibre direction in (H), normal and (I) early degenerate cartilage.

Discussion

The superficial zone of articular cartilage has several unique structural features and here we have combined mechanical loading with multiphoton microscopy to investigate the role these play in its mechanical properties.

We began by determining tensile and compressive moduli and Poisson's ratios. At the whole-sample level our data were consistent with previous measurements. However the tensile moduli of 14MPa parallel and 8MPa perpendicular was lower than previously reported values for the superficial zone of equine cartilage (43MPa parallel and 18MPa perpendicular [21]). This discrepancy is probably because our cartilage strips were approximately 500μm thick which is greater than the superficial zone thickness in equine cartilage (50-100μm) and therefore contained some of the more compliant deeper zone. At strains greater than 5% the Poisson's ratios for the superficial zone are comparable with those of Elliot et al (1.87±1.11) [38] but larger than those of Huang et al [22] (0.95-1.16) (both in human cartilage). We noted that the highest values for the Poisson's ratio occurred in the upmost 25μm. The lower values calculated by Huang et al were from 250μm thick strips of superficial zone cartilage, so the discrepancy may reflect a gradient in Poisson's ratio with depth. The Poisson's ratios for both tensile and compressive loading showed that water was lost from the cartilage, this is important to measure as it indicates the role of proteoglycans in the mechanical properties and affects the osmotic environment surrounding the cells and changes in cell volume [39].

On a smaller scale there were substantial heterogeneities in the responses to both tensile and compressive loads, which can be related to variations in tissue structure and composition. Under tensile load the strain distribution was heterogeneous both with depth and within the plane parallel to the articular surface. Tensile forces are largely resisted by the collagen fibres and the heterogeneities supported the suggestion that collagen is arranged in leaflets (as illustrated in figure 1B). However, the behaviour may also be dependent on the proteoglycan distribution. The proteoglycan concentration is lower in the superficial zone than in deeper regions and consequently water is lost more easily. [16] The swelling pressure is the major determinant of the response to compressive loads and this is supported by our observation of a vertical gradient in compressive modulus, but no significant lateral variation.

Under both tensile and compressive load there was a wide scatter in the responses of individual cells, raising questions about the validity of assuming that cells within a given zone of articular

cartilage experience the same mechanical loading. More detailed studies of the structural and metabolic responses of individual cells are required. Chondrocyte behaviour is known to be dependent on mechanical loading [40] however the exact mechanisms for cell strain sensing are not fully understood. Imaging the deformations of the cells and matrix under loads should be informative especially for assessing the role of organelles such as the primary cilium [41].

The cellular deformations were measured 30 minutes after loading and most likely represent the equilibrium response. These values will provide a baseline for more physiological dynamic studies as well as being directly relevant to cases of long term bed-rest and immobilised joints. Experiments on isolated chondrocytes have demonstrated their ability to regulate their cytoplasmic volume in response to changes in osmotic environment [42]. Similar measurements in loaded tissue would help establish whether the presence of the extracellular matrix, acting both as a determinant of external osomotic pressure and as a mechanical support, influences the extent and time-course of such processes.

This study focused on the elastin network. We believe we have demonstrated that elastin fibres do not passively follow the deformation of the surrounding matrix and that they are under tension even in the absence of external load. As the elastin fibres lie in the plane parallel to the articular surface they show minimal deformation under compressive loads. Their role is most likely to aid the recovery of cartilage after shear and tensile loading. Shear and tensile forces are highest close to the articular surface where the density of elastin fibres is greatest and where rehydration-forces generated by the proteoglycans are at a minimum.

Corrugations at the surface were observed under high tensile strains and although it is not possible to establish whether these could occur *in vivo* it is a further demonstration of the complexity of surface micromechanics and the presence of pre-stress in the intact tissue. Though the combination of mechanical forces required to produce corrugations is unclear, we have demonstrated they generate irregular strain fields within the most superficial 0-30μm and have a striking effect on the morphology of individual cells which might have profound metabolic consequences, perhaps in the initiation of degenerative processes.

This study revealed microscopic lesions in some samples which appeared macroscopically normal. These lesions opened up under tensile load and their behaviour appears to fit closely with one of the earliest degenerative changes associated with OA, “cartilage softening”. This occurs prior to extensive fibrillation of the articular surface and corresponds to a decrease in connectivity of the

collagen network as illustrated in figure 8H and I [43-45]. We speculate that the splits opening up parallel to the collagen fibre direction are due to this early loss of connectivity.

Multiphoton microscopy provides detailed data, which can be readily segmented to form inputs for mechanical models [46]. When this is combined with mechanical testing as shown here it provides a valuable resource for theoretical cartilage micromechanics studies, allowing iterative comparisons of experimental mechanical tests within cartilage with biologically informed finite element models.

Author contributions:

Jessica Mansfield was responsible for the experimental work and data analysis. James Bell contributed to the experimental work and data analysis and interpretation. Peter Winlove, was responsible for overseeing the project. All authors contributed to analysis and interpretation of the results, drafting, editing and final approval of the manuscript.

Funding source:

This work was funded by Arthritis Research UK Grant No. 19432.

Competing Interests:

There are no competing interests for this research

References:

1. Stockwell RA. Biology of Cartilage Cells, Cambridge University Press 1979.
2. Benninghoff A. Form und bau der Gelenknorpel in ihren Bezeihungen zur Function. Z Zellforsch Mikrosk Anatomy 1925; 2: 783-825.
3. Maroudas A. Balance between swelling pressure and collagen tension in normal and degenerate cartilage. Nature 1976; 260: 808-809.
4. Chen SS, Falcovitz YH, Schneiderman R, Maroudas A, Sah RL. Depth-dependent compressive properties of normal aged human femoral head articular cartilage: relationship to fixed charge density. Osteoarthritis and Cartilage 2001; 9: 561-569.
5. Yeh AT, Hammer-Wilson MJ, Van Sickle DC, Benton HP, Zoumi A, Tromberg BJ, et al. Nonlinear optical microscopy of articular cartilage. Osteoarthritis and Cartilage 2005; 13: 345-352.
6. Yu J, Urban JPG. The elastic network of articular cartilage: an immunohistochemical study of elastin fibres and microfibrils. Journal of Anatomy 2010; 216: 533-541.
7. Mansfield JC, Yu J, Attenburrow DP, Moger J, Tirlapur U, Urban JPG, et al. The elastin network: its relationship with collagen and cells in articular cartilage as visualized by multiphoton microscopy. Journal of Anatomy 2009; 215: 682-691.
8. Hesse I. The Occurrence of Elastic System Fibers in the Matrix of Normal Articular-Cartilage. Cell and Tissue Research 1987; 248: 589-593.
9. He B, Wu JP, Chim SM, Xu J, Kirk TB. Microstructural analysis of collagen and elastin fibres in the kangaroo articular cartilage reveals a structural divergence depending on its local

mechanical environment (vol 21, pg 237, 2013). Osteoarthritis and Cartilage 2013; 21: 237-245
10. Poole CA. Articular cartilage chondrons: Form, function and failure. Journal of Anatomy 1997; 191: 1-13.
11. Mansfield J, Moger J, Green E, Moger C, Winlove CP. Chemically specific imaging and in-situ chemical analysis of articular cartilage with stimulated Raman scattering. Journal of Biophotonics 2013; 6: 803-814.
12. Wong M, Wuethrich P, Eggli P, Hunziker E. Zone-specific cell biosynthetic activity in mature bovine articular cartilage: A new method using confocal microscopic stereology and quantitative autoradiography. Journal of Orthopaedic Research 1996; 14: 424-432.
13. Vanderploeg EJ, Wilson CG, Levenston ME. Articular chondrocytes derived from distinct tissue zones differentially respond to in vitro oscillatory tensile loading. Osteoarthritis and Cartilage 2008; 16: 1228-1236.
14. Choi JB, Youn I, Cao L, Leddy HA, Gilchrist CL, Setton LA, et al. Zonal changes in the three-dimensional morphology of the chondron under compression: The relationship among cellular, pericellular, and extracellular deformation in articular cartilage. Journal of Biomechanics 2007; 40: 2596-2603.
15. Venn M, Maroudas A. Chemical composition and swelling of normal and osteoarthrotic femoral head cartilage. I. Chemical composition. Annals of the Rheumatic Diseases 1977; 36: 121-129.
16. Torzilli PA, Dethmers DA, Rose DE, Schryuer HF. Movement of Interstitial Water through Loaded Articular- Cartilage. Journal of Biomechanics 1983; 16: 169-179.
17. McCutchen CW. The frictional properties of animal joints. Wear 1962; 5: 1-17.
18. Neu CP, Hull ML, Walton JH. Heterogeneous three-dimensional strain fields during unconfined cyclic compression in bovine articular cartilage explants. Journal of Orthopaedic Research 2005; 23: 1390-1398.
19. Woo SLY, Akeson WH, Jemmott GF. measurements of nonhomodeneous directional mechanical properties of articular cartilage in tension. Journal of Biomechanics 1976; 9: 785-791.
20. Kempson G, Freeman M, Swanson S. Tensile properties of articular cartilage. Nature 1968; 220: 1127-1128.
21. Bell JS, Christmas J, Mansfield JC, Everson RM, Winlove CP. Micromechanical response of articular cartilage to tensile load measured using nonlinear microscopy. Acta Biomaterialia 2014; 10: 2574-2581.
22. Huang CY, Stankiewicz A, Ateshian GA, Mow VC. Anisotropy, inhomogeneity, and tension-compression nonlinearity of human glenohumeral cartilage in finite deformation. Journal of Biomechanics 2005; 38: 799-809.
23. Akizuki S, Mow V, Müller F, Pita J, Howell D, Manicourt D. Tensile properties of human knee joint cartilage: I. Influence of ionic conditions, weight bearing, and fibrillation on the tensile modulus. Journal of Orthopaedic Research 1986; 4: 379-392.
24. Roth V, Mow V. The intrinsic tensile behavior of the matrix of bovine articular cartilage and its variation with age. The Journal of Bone and Joint Surgery 1980; 62: 1102-1117.
25. Kempson G. Relationship between the tensile properties of articular cartilage from the human knee and age. British Medical Journal 1982; 41: 508-511.
26. Diaspro A, Sheppard CJR. Two-Photon Excitation Flouresence Microscopy. In: Confocal and Two-Photon Microscopy: Foundations, Applications and Advances, Diaspro A Ed.: Wiley-Liss Inc. 2002:39-73.
27. Freund I, Deutsch M, Sprecher A. Connective-Tissue Polarity - Optical 2nd-Harmonic Microscopy, Crossed-Beam Summation, and Small-Angle Scattering in Rat-Tail Tendon. Biophysical Journal 1986; 50: 693-712.

28. Mansfield JC, Winlove CP, Moger J, Matcher SJ. Collagen fiber arrangement in normal and diseased cartilage studied by polarization sensitive nonlinear microscopy. Journal of Biomedical Optics 2008; 13: 044020.
29. Mansfield JC, Winlove CP. A multi-modal multiphoton investigation of microstructure in the deep zone and calcified cartilage. Journal of Anatomy 2012; 220: 405-416.
30. Alkhouli N, Mansfield J, Green E, Bell J, Knight B, Liversedge N, et al. The Mechanical Properties of Human Adipose Tissues and their Relationships to the Structure and Composition of the Extracellular Matrix. American journal of physiology. Endocrinology and metabolism 2013; 305: 1427-1435.
31. Chen H, Liu Y, Slipchenko MN, Zhao XF, Cheng JX, Kassab GS. The Layered Structure of Coronary Adventitia under Mechanical Load. Biophysical Journal 2011; 101: 2555-2562.
32. Liang X, Graf BW, Boppart SA. In Vivo Multiphoton Microscopy for Investigating Biomechanical Properties of Human Skin. Cellular and Molecular Bioengineering 2011; 4: 231-238.
33. Wan W, Dixon JB, Gleason RL. Constitutive Modeling of Mouse Carotid Arteries Using Experimentally Measured Microstructural Parameters. Biophysical Journal 2012; 102: 2916-2925.
34. Rasband W. Image J. National Institutes of Health USA.
35. Christmas J, Everson RM, Bell JS, Winlove CP. Inexact Bayesian point pattern matching for linear transformations. Pattern Regonition 2014; 47: 3265-3275.
36. Clarke I. Articular cartilage: a review and scanning electron microscope study: 1. The interterritorial fibrillar architecture. Journal of Bone and Joint Surgery-British Volume 1971; 53: 732-750.
37. Sasazaki Y, Shore R, Seedhom BB. Deformation and failure of cartilage in the tensile mode. Journal of Anatomy 2006; 208: 681-694.
38. Elliott DM, Narmoneva DA, Setton LA. Direct measurement of the Poisson's ratio of human patella cartilage in tension. Journal of Biomechanical Engineering 2002; 124: 223-228.
39. Urban J. The chondrocyte: a cell under pressure. Rheumatology 1994; 33: 901-908.
40. Grodzinsky AJ, Levenston ME, Jin M, Frank EH. Cartilage tissue remodeling in response to mechanical forces. Annual Review of Biomedical Engineering 2000; 2: 691-713.
41. Poole CA, Flint MH, Beaumont BW. Analysis of the morphology and function of primary cilia in connective tissues:A cellular cybernetic probe? Cell Motility 1985; 5: 175-193.
42. Bush PG, Hall AC. Regulatory volume decrease (RVD) by isolated and in situ bovine articular chondrocytes. Journal of cellular physiology 2001; 187: 304-314.
43. Chen MH, Broom N. On the ultrastructure of softened cartilage: a possible model for structural transformation. Journal of Anatomy 1998; 192: 329-341.
44. Chen MH, Broom ND. Concerning the ultrastructural origin of large-scale swelling in articular cartilage. Journal of Anatomy 1999; 194: 445-461.
45. Broom N, Chen MH, Hardy A. A degeneration-based hypothesis for interpreting fibrillar changes in the osteoarthritic cartilage matrix. Journal of Anatomy 2001; 199: 683-698.
46. Lilledahl M, Pierce D, Ricken T, Holzapfel G, de Lange Davies C. Structural Analysis of Articular Cartilage Using Multiphoton Microscopy: Input for Biomechanical Modeling. IEEE Transactions on Medical Imaging 2011; 30: 1635-1648.

1 Supplementary information:

Supplementary Information showing the anatomy of the equine metacarpophalangeal joint, the split line directions on the proximal phalanx and the regions form which both parallel and perpendicular cartilage strips were taken for tensile loading

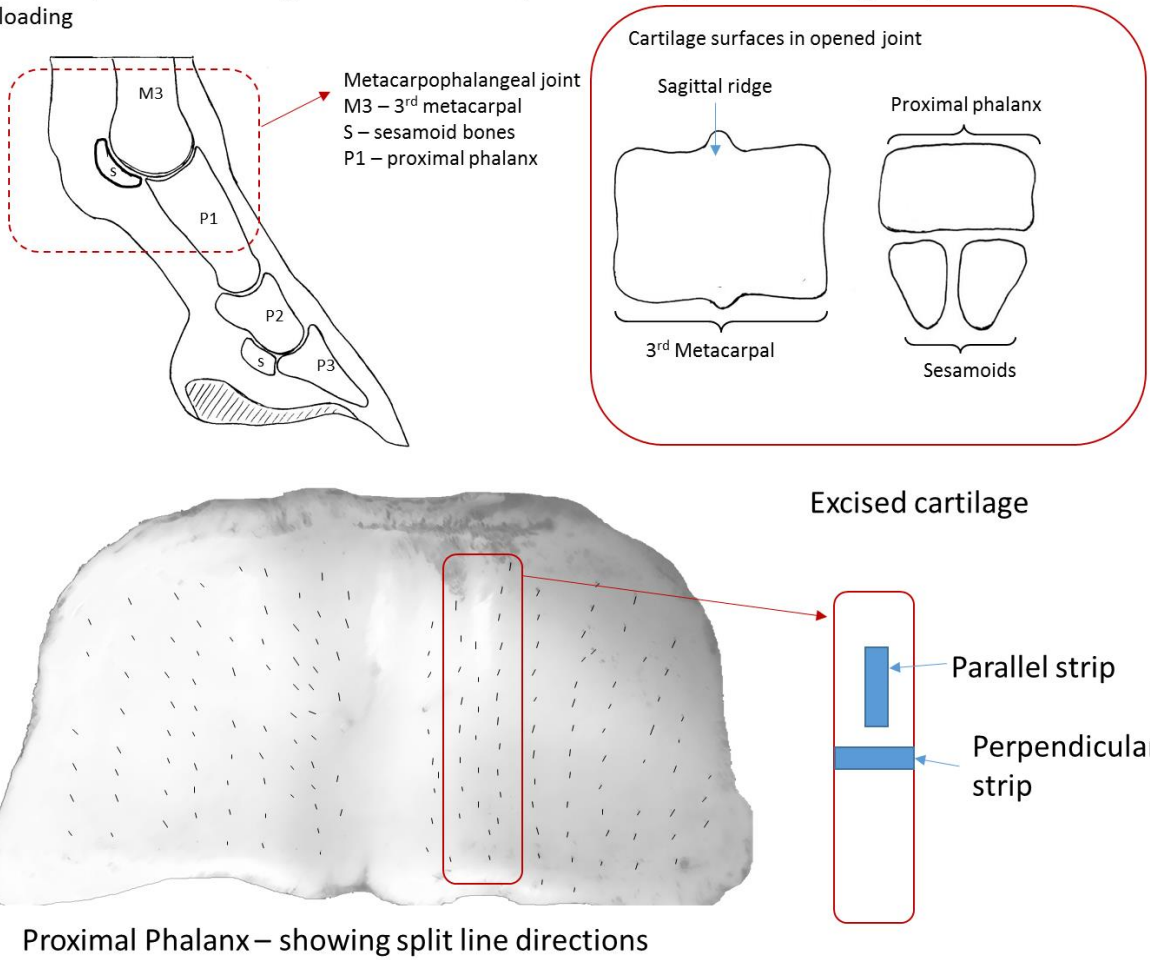

Proximal Phalanx – showing split line directions

2
3